Tectonophysics 609 (2013) 423–436

Contents lists available at ScienceDirect

Tectonophysics

journal homepage: www.elsevier.com/locate/tecto

Review Article

Imaging and observing the electrical Moho

Alan G. Jones *

Dublin Institute for Advanced Studies, Ireland

ARTICLE INFO

Article history:
Received 18 July 2012
Received in revised form 6 February 2013
Accepted 14 February 2013
Available online 26 February 2013

Keywords:
Moho
Electrical Moho
Electrical conductivity
Electrical resistivity
Crust–mantle boundary

ABSTRACT

Defining the depth to the base of the crust is of profound importance for understanding and developing theories of the secular variation of our planet, including crustal formation and evolution. Since its discovery 100 year ago, the seismic Moho is, almost ubiquitously, used as the crust–mantle boundary reference. Laboratory studies on crustal and mantle rocks suggest that there should be a concomitant step-lie change in electrical conductivity, an electric Moho (eMoho), at the crust–mantle boundary. We examine resolution properties of electrical and electromagnetic methods for imaging and observing an eMoho for three generic models, one to represent the Archean, one for the Proterozoic, and the third for the Phanerozoic. We show that in all three cases, given the existence in most localities of a conducting lower crust compared to the upper crust and upper lithospheric mantle, the problem is difficult and at the edge, and often beyond, confident resolution. For some highly unusual localities however, the lower crust is more resistive than the underlying upper mantle, and in those cases it is possible to resolve an eMoho, but very high quality data are required. Examples of eMoho observations around the globe are discussed, focussing on the results from a site on the southwestern part of the Slave Craton, northwestern Canada.

Contents

1. Introduction

One hundred years ago, Mohorovičić (1910) analysed data from an earthquake near Pokupsko, 40 km south-east of Zagreb, and discovered a dramatic increase in compressional seismic velocity, from a velocity of 5.68 km/s to 7.75 km/s, at a depth of 54 km beneath the Kulpa Valley in

* Tel.: +353 1 653 5147 x200; fax: +353 1 443 0575.
E-mail address: alan@cp.dias.ie.

0040-1951/$ – see front matter © 2013 Elsevier B.V. All rights reserved.
http://dx.doi.org/10.1016/j.tecto.2013.02.025

Croatia. Since that serendipitous discovery, the "Moho" has become arguably the most important seismological horizon of both the oceans and continents owing to its adopted role in defining the crust–mantle boundary. It is a ubiquitous feature of the Earth, and is commonly assumed to separate lower-crustal silica-rich mafic granulite rocks from higher velocity (typically >8 km/s) upper-mantle olivine-dominated ultramafic peridotite rocks. There does though continue to be long-standing debate about the differing elastic (Moho) and petrological definitions of the crust–mantle boundary as eclogite, a crustal rock, can have high (mantle-like) velocity (e.g., Mengel and Kern, 1992). That debate is though immaterial for this paper, where we define an electrical expression of the petrological crust–mantle boundary as the eMoho.

Since that observation, various other seismic Mohos have been defined, including a refraction Moho, a reflection Moho and a teleseismic Moho (see Eaton, 2006 and references therein). These Mohos are all reviewed in Cook et al.'s (2010) study, and particularly the reflection and refraction Mohos are compared and contrasted and shown statistically to be in the main consistent but with significant departures for some areas of Canada.

This paper concerns itself with an electrical manifestation of a crust–mantle signature, the eMoho, given by a step-like change in electrical conductivity characteristics. In the following Section, the existence of an eMoho is discussed, followed by the abilities of various electrical and electromagnetic methods to sense the eMoho. Subsequently, observations of the eMoho are reviewed — these are few, for the reasons outlined below, but nevertheless significant. Finally, recommendations are drawn for advancing our knowledge of the eMoho.

2. Existence of an eMoho

Is there a reason to expect a step change in conductivity at the crust–mantle boundary? Petrologically, the crust–mantle boundary separates silica-rich felsic and mafic crustal rocks from ultramafic peridotitic rocks below (Mengel and Kern, 1992). If dry and absent of any minor conducting phase, then laboratory studies suggest that there should be an increase in electrical resistivity, i.e., a decrease in electrical conductivity, transitioning from lower crustal mafic rocks to upper mantle ultramafic rocks. A compilation of laboratory studies by Kariya and Shankland (1983) shows that dry lower crustal mafic rocks are of the order of some 1000–40,000 Ω m, with high values (tens of thousands of Ω m) for low temperatures expected in Precambrian strata (400–500 °C), and low values (thousands of Ω m) for warmer temperatures in Phanerozoic strata (500–800 °C). Silicic rocks are more resistive, interpreted to be due to lower iron content (Kariya and Shankland, 1983). In contrast, dry peridotite at uppermost mantle temperatures (400–500 °C for Precambrian regions and 500–800 °C for Phanerozoic regions) is highly resistive, with the most complete olivine model for polaron conduction, SE03 of Constable (2006), suggesting resistivities of the order of 5.5×10^5–10^6 Ω m. Whole rock calculations based on expected compositions of olivine, ortho- and clino-pyroxene and spinel, yield values not much different (Fullea et al., 2011; Jones et al., 2009a), given the dominance of olivine in the matrix and that the second most common mineral, orthopyroxene, has an electrical conductivity very similar to that of olivine.

Thus, for totally dry lower crust and uppermost mantle, there can be expected to be at least an order of magnitude increase in resistivity at the eMoho. However, rarely are the lower crust or the uppermost mantle found be to as resistive as expected, with contributions from water, sulphides, iron oxides and graphite proposed for the conducting lower crust, and the role of proton conduction from hydrogen diffusion being dominant in the upper mantle (Jones et al., 2012; Jones et al., 2013; Karato, 1990). Even with 100 wt ppt water in olivine and for reasonable assumptions about mineral composition, the resistivity at 400–500 °C at the top of the mantle lithosphere is expected to be of the order of 5×10^4–5×10^5 Ω m, so still providing a resistivity increase at the eMoho. For Phanerozoic strata, the expected resistivity for rocks comprising 75% wet olivine is of the order of 600–6000 Ω m at temperatures of 600–800 °C, providing for a smaller contrast to dry lower crust. However, Phanerozoic regions all have a conducting lower crust of resistivity less than 100 Ω m; or rather, there is not one single reported case of an MT study over a Phanerozoic region that has reported resistive lower crust, so there is expected to be an order of magnitude or more increase in resistivity.

3. Imaging the eMoho

3.1. Electrical and electromagnetic methods

There are two different physical approaches for imaging electrical conductivity, namely conductive and inductive methods. Conductive methods are DC resistivity, dipole–dipole, etc., whereas inductive methods are magnetotellurics (MT) and controlled-source electromagnetics (CSEM), where the latter can have various geometries and types of sources (horizontal or vertical magnetic loops or horizontal electric bipole) and receivers (three components of the magnetic field and/or the two horizontal components of the electric field). In the following, we will consider a Wenner-style DC resistivity array, standard MT, and a grounded-bipole CSEM source.

3.2. Generic models of the continental lithosphere

For the purposes of this examination, let us define three types of generic continental lithosphere, one we will call "Archean", the second "Proterozoic", and the third we will call "Phanerozoic". The essential differences between the three are (1) the thickness of the crust, (2) the conductance of the lower crust, and (3) the depth to the lithosphere–asthenosphere boundary (LAB, added for completeness, as the periods sensing the eMoho and the LAB are distinctly different for thick lithosphere, but there is overlap for thin lithosphere). We divide the crust into two layers, the upper crust and the lower crust, both of equal thickness. Archean and Proterozoic lithospheres have an assumed crust–mantle boundary at 40 km, whereas for Phanerozoic lithosphere it is assigned at a depth of 35 km.

There is a wide variety of models that can be explored, from 1D ones of many layers to 2D and 3D ones with lateral heterogeneity. Of course, in reality the crust is in most places far more complex than two layers, but for the purposes of this simple examination two layers suffice. Any more complexity in the crust will result in lower resolution of the eMoho than can be achieved with only two isotropic crustal layers, and the point here is to examine resolution properties in best-case scenarios. Also, note that none of these generic models have any thick sedimentary cover on top of them. Should there be cover, then resolution will decrease markedly (see, e.g., Jones, 1992, Fig. 3–8). All of the generic models have a resistivity increase at the eMoho, as this is the most likely scenario given petrological and mineralogical arguments. When we examine the results for the southern part of the Slave Craton, we will discover that the generic Archean model does not represent the Slave Craton at all, in that there is a highly anomalous resistivity decrease at the eMoho for that region which facilitates resolution of the eMoho.

For the lower crust, as noted 20 years ago by Jones (1981) and later expanded upon by Haak and Hutton (1986), Hyndman and Shearer (1989), Jones (1992) and Shankland and Ander (1983), global compilations show that there is generally an age-progression of the total conductance of the continental lower crust, with younger (Phanerozoic to recent) regions exhibiting a conductance (depth-integrated conductivity, σh) of the order of 200–2000 S, and older (Precambrian) regions exhibiting a conductance of the order of 2–20 S. The reasons for the existence of the enhanced conductivity in the continental lower crust are still not established and remain an issue of intense

debate (Frost et al., 1989; Jones, 1992; Yang, 2011; Yardley and Valley, 1997; Yoshino and Noritake, 2011), but it is not relevant for this paper.

For the LAB, Archean cratons have typically 200–250 km thick lithospheres, Proterozoic ones have 150–200 km thick lithospheres, and Phanerozoic regions have 80–120 thick lithospheres (for a discussion of the European LAB, see Jones et al., 2010). Again, these are generic thicknesses that are representative of global compilations. There may be anomalous regions where the Proterozoic LAB is thicker than the Archean LAB.

The electrical parameters (resistivities and thicknesses) of the three lithospheres and underlying asthenosphere, in terms of 5 (Phanerozoic) or 6 (Proterozoic and Archean) discrete layers, are given in Table 1. We are assuming a uniform isotropic resistivity value for each crustal and mantle layer and for the asthenosphere. There is a very resistive upper crust for the Archean model (40,000 Ω m), a high resistivity for the Proterozoic model (10,000 Ω m), and a moderate resistivity for the Phanerozoic model (1000 Ω m). This variation is in accord with observations generally, but again there can be regions that do not display such distinctions. The lower crustal resistivity is given by the thickness divided by the assumed conductances of 2 S, 20 S and 200 S for the Archean, Proterozoic and Phanerozoic models respectively. These conductance values are consistent with the statistics of observations of the lower crust (Hyndman and Shearer, 1989; Jones, 1992).

The mantle lithosphere is divided into two (Phanerozoic) or three (Proterozoic and Archean) layers. For the Archean and Proterozoic models, the uppermost layer has a resistivity of 50,000 Ω m to a depth of 80 km, i.e., 40 km thickness, below which is a layer of 5000 Ω m to either 150 km (Archean) or 130 km (Proterozoic). The single upper mantle lithosphere layer is 35 km thick for the Phanerozoic model, and of 5000 Ω m. The lower lithosphere for all models, to the LAB, has a resistivity of 500 Ω m. In reality, the mantle lithospheric resistivity will vary continuously with depth, such that log (resistivity) decreases linearly, consistent with the exponential thermal sensitivity in the Arrhenius equation describing polaron conduction, from an initial value well in excess of 100,000 Ω m to a value of 100 Ω m at the LAB, which is the expected resistivity value for olivine-dominated rocks at a temperature of 1350 °C. We are approximating this decrease by two or three layers, which is sufficient for the purposes of this paper. Note that for completeness we should take iron content into account, and have a more depleted upper mantle beneath the Archean model (Mg# of 93), an intermediate value for Proterozoic mantle (Mg# of 91) and fertile mantle beneath the Phanerozoic model (Mg# of 89). However, the effects of these variations in iron content are negligible compared to the temperature effects. Note also that we are omitting the effects of water, known to enhance conductivity in the mantle since Karato's (1990) paper, as discussed recently in Jones et al. (2012, 2013). We assign the asthenosphere a resistivity of 10 Ω m, which is the median value of the globally observed range for the asthenosphere of 5–25 Ω m (see, e.g., Jones, 1999).

The three models are shown in Fig. 1. For the problem at hand, which is to resolve the depth to the base of the crust, the eMoho, our main priority is to determine the sum of the thicknesses of the top two layers, $h_1 + h_2$, where layers 1 and 2 are the upper crust and lower crust respectively. A simple method for illustrating sensitivity to eMoho depth is to vary the crustal thickness parameters and inspect the differences in responses derived. This is undertaken for each method by changing the eMoho depth by ±20%, which is achieved in all cases by reducing or increasing the thickness of the lower crustal layer. Thus, the Archean and Proterozoic models tested are for an eMoho at 32 km and 48 km, with a lower crustal layer of 12 km and 28 km respectively. For the Phanerozoic model, the eMoho ranges from 28 km to 42 km, with the lower crustal layer of 10.5 km and 25.5 km respectively. Another test can be made for resolution problems associated with equivalency, a well-known problem in electrical and EM methods. In this test, the conducting lower crust is replaced by a layer with exactly the same conductance, but with half the resistivity and half the thickness.

In all geophysical methods however, the model parameters that we define to describe the Earth, usually a physical parameter (e.g., conductivity, density, velocity, etc.) and one or more lengths (thickness, distance), are not those that are resolved, due to non-uniqueness and equivalence of models. To inspect resolution properties, it is necessary to orthonormalize the model parameters into their eigenparameter combinations using a singular value decomposition (SVD) of the system matrix of partial derivatives (Jacobian) between the model parameters and the data (Edwards et al., 1980; Edwards et al., 1981; Ilkisik and Jones, 1984; Inman, 1975; Jones, 1982; Wiggins, 1972). Using an SVD sensitivity analysis for generic electrical models of the continental lithosphere, we examine the resolution of the depth to the base of the crust for different electrical and electromagnetic techniques, and for different errors. The MT results are examined in greatest detail, as the technique has been applied far more broadly than the others given the cost of acquisition, the simplicity of the logistics and the more advanced processing and modelling tools.

3.3. DC technique

There are various configurations of DC resistivity methods, the three main ones being Wenner, Schlumberger and dipole–dipole, and all of them are related to each other; that is, one can convert one response into another using mathematical formulae. We consider here the Wenner configuration, as it has the greatest vertical resolution of the standard arrays (Roy and Apparao, 1971). In the Wenner configuration, the four electrodes are spaced equidistantly with the outer two as the source electrodes and the inner two as the receiver (potential) electrodes. The depth of penetration is approximately 1/10th (standard Wenner) to 1/5th (Wenner-β and Wenner-γ) of the potential electrode separation (Szalai et al., 2009). Hence, to sense the eMoho at a depth of 40 km for the standard Wenner array the electrode spacing must be on the order of 400 km, with the current electrodes 3 times that apart, i.e., 1200 km. We recognise that logistically the Wenner configuration requires the greatest field effort and is the most cumbersome to implement. Indeed, no deep-sensing DC experiments have used the Wenner configuration. However, we wish to examine the method with the greatest potential for resolution, as any other method will, of necessity, have worse resolution.

The apparent resistivities that would be measured on the three generic models are shown in Fig. 2 (thick lines). The sensitivity tests for the depth to the eMoho, assuming that the lower crustal layer changes in thickness to result in ±20% variation in the eMoho, are also shown in Fig. 2 (thin lines). There is clearly sensitivity for

Table 1
Model parameters.

Model	Upper crust		Lower crust		Mantle lithosphere		Asthenosphere
	Resistivity (Ω · m)	Thickness (km)	Resistivity (Ω · m)	Thickness (km)	Resistivity (Ω · m)	Thickness (km)	Resistivity (Ω · m)
Archean	40,000	20	10,000	20	50,000/5000/500	40/70/75	10
Proterozoic	10,000	20	1000	20	50,000/5000/500	40/50/45	10
Phanerozoic	1000	17.5	87.5	17.5	5000/500	35/25	10

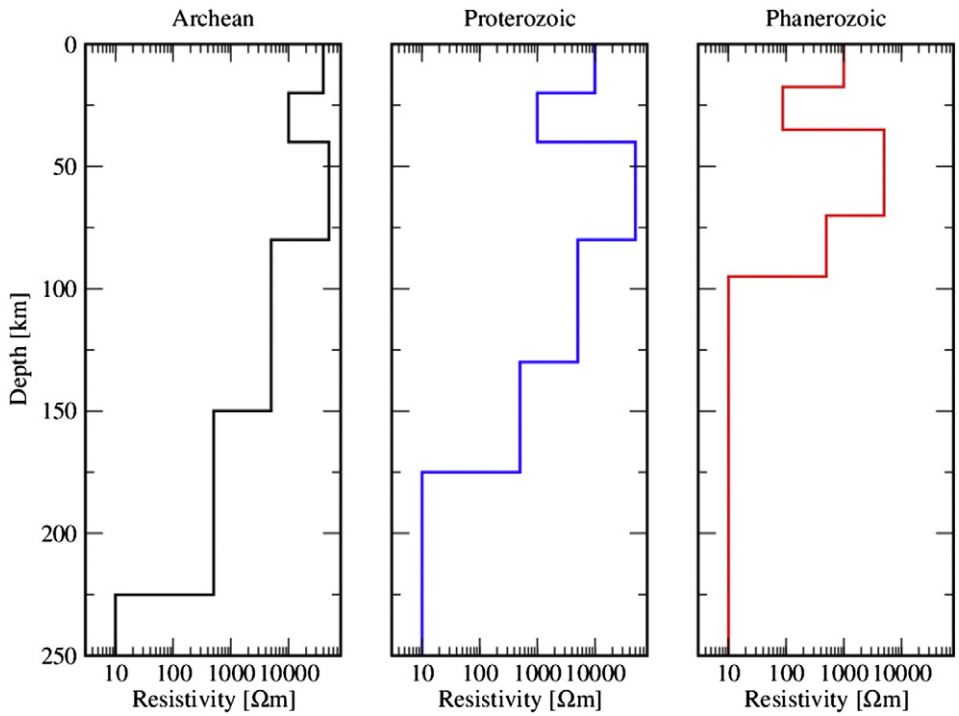

Fig. 1. Generic electrical models of the continental lithosphere beneath Archean, Proterozoic and Phanerozoic regions.

electrode spacing greater than around 50 km, i.e., total current electrode spread length of 150 km.

One well-known problem with DC resistivity techniques is equivalency, i.e., virtually the same responses can be obtained from a number of models (see Parker, 1984; and discussion and references in Szaraniec, 1986). In all three cases studied, we have a resistive upper crust, a more conducting lower crust, and a resistive mantle, the so-called H-type case. We can test equivalency for the conducting lower crust by alerting it but keeping the conductance the same. The responses from models with a lower crust with thicknesses and resistivities that are half of those of the standard generic models are shown in Fig. 3, where the full lines are the generic models' responses, and the dashed lines are those of the altered models.

Clearly, there is, within typical data errors, virtually complete equivalency and the actual thickness of the conducting lower crust cannot be determined from DC measurements. Only at very large distances, of the order of 150 km electrode separation which is a 450 km spread length, is there even the remote chance of resolving equivalency. However, the Earth must be uniform over those length scales, and also there cannot be any 3D conducting effects that channel current in the near-surface. Those problems are discussed below in the field examples.

3.4. MT technique

In the absence of error and for continuous data at all frequencies, there exists only one MT model that will fit the responses (Bailey, 1970)9. This uniqueness theorem, absent in other potential field integrating methods in geophysics, is a powerful statement and drives us to acquire higher and higher quality data. Non-uniqueness is thus a consequence of data error and data insufficiency, i.e., not broad enough period band and not enough points per decade. If the data

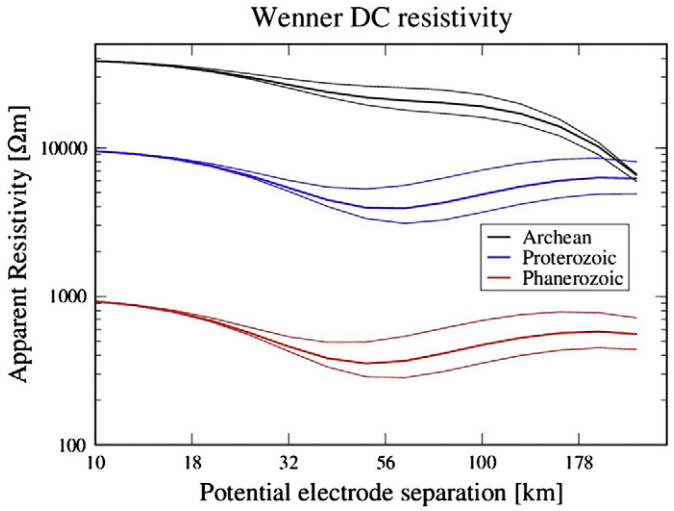

Fig. 2. DC resistivity responses for the models shown in Fig. 1. The thin lines are for the lower crustal thickness altered such that the Moho depth varied by 20%.

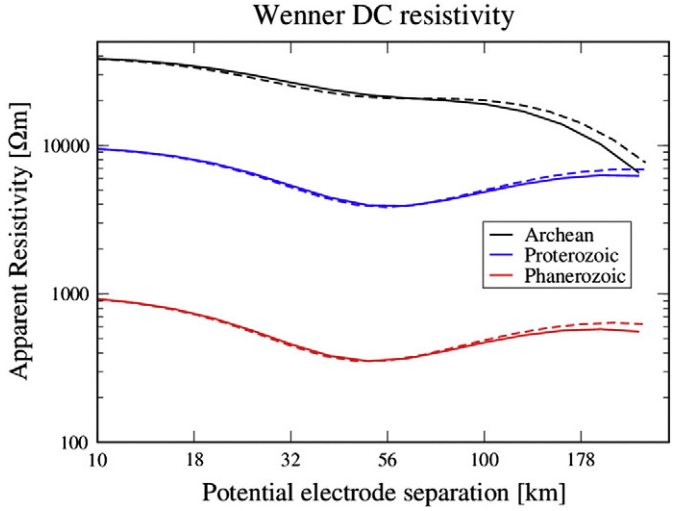

Fig. 3. DC resistivity responses for the models shown in Fig. 1 (full lines) together with the responses for the equivalency models (dashed lines).

are of limited period band, then the uppermost part is not resolved as well as possible given the lack of high frequency information, and similarly the lowermost part is not resolved as well as possible given the lack of low frequency data. The more estimates per decade one has, then the greater resolution one has, assuming of course that all estimates are independent of each other and that neither the spectral windowing function nor the estimation technique has led to dependence between neighbouring estimates.

The physics of magnetotellurics is such that there is assumed a plane wave incident on the Earth's surface that induces only toroidal current systems which flow within horizontal planes in a 1D layered Earth. One consequence of this is that, for discrete data with error, the best-fitting model to a 1D MT response is given by a series of delta-like conductance spikes (Parker, 1980). (As an aside, this latter result is being used as a tool to check the internal consistency between the apparent resistivity data and the phase data (Parker and Booker, 1996), see, for example, Spratt et al. (2005)) Thus, the model parameters that describe conductive layers sandwiched between resistive ones, namely the thickness h and conductivity σ, are combined to form the eigenparameter that describes the vertically-integrated conductivity, conductance S, given by $S = \sigma h = h/\rho$.

The MT responses that would be observed for the three models in the period range of 0.01–1000 s are shown in Fig. 4 (thick lines), together with the responses for models with the eMoho at ±20% depths (thin lines).

As with DC resistivity, there is a strong equivalency of responses between models that have the same conductance. This can be illustrated by considering the equivalency models, where the conductance of the lower crust remains the same, but the conductivity is doubled (resistivity halved) and the thickness halved. The responses from those equivalency models are shown in Fig. 5 (dashed lines).

Examining the three models for very low noise levels (1% in impedance, equivalent to 0.58° in the phase and 2% in the apparent resistivity), by adding Gaussian distributed noise and scatter to the impedance estimates and to the error estimates, gives the SVD eigenparameters ordered as listed in Table 2 (Archean), Table 3 (Proterozoic) and Table 4 (Phanerozoic). For each model the residual effective degrees of freedom, which define how many eigenparameters are resolved, are listed together with the fractional error associated

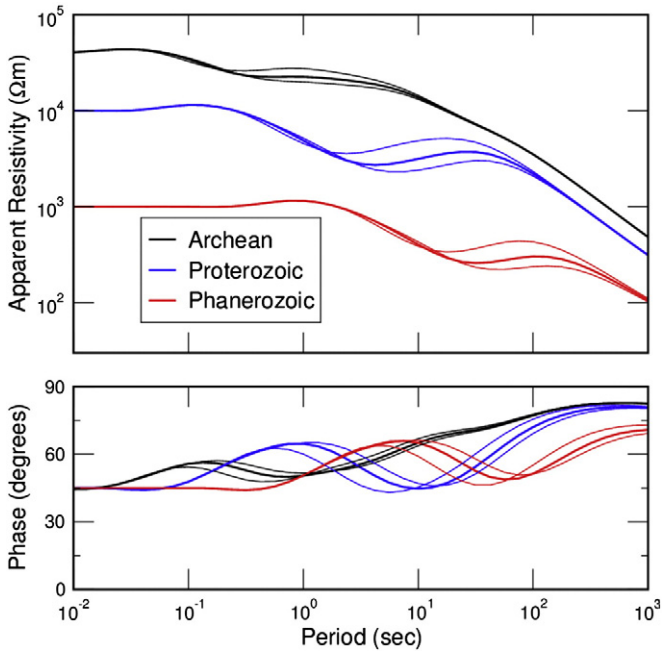

Fig. 4. MT responses for the models shown in Fig. 1. The thin lines are for the lower crustal thickness altered such that the Moho depth varied by 20%.

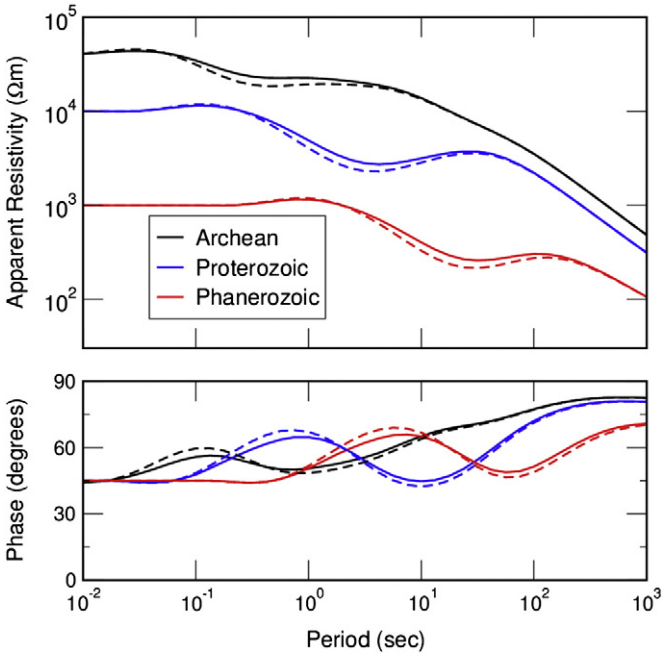

Fig. 5. MT responses for the models shown in Fig. 1 (full lines) together with the responses for the equivalency models (dashed lines).

with that particular eigenparameter. The unresolved parameters, in all cases, for this level of noise are the resistivities of the mantle lithospheric layers. This is a well-known resolution issue in MT for resolving the absolute resistivity of a resistive layer sandwiched between two conducting ones (see, e.g., Jones, 1999). Although the conductance (vertically-integrated conductivity) of a conducting layer sandwiched between two more resistive ones is well resolved, the resistance (vertically-integrated resistivity) R, given by $R = \rho\, h = h/\sigma$, is a very difficult to determine eigenparameter. All other parameters are resolved to better or lesser degrees.

As noise levels increase however, the number of degrees of freedom, i.e., the number of resolved eigenparameters, decreases. This is illustrated in Fig. 6 for noise levels from 1% to 16% added to the impedance values. The integrated resistivity of the lower crust (i.e., $R_2 = \rho_2 h_2$) becomes unresolved as noise increases, and if R_2 is not resolved, then only S_2 is resolved and the actual value of h_2 is not independently resolved.

Finally, the number of estimates per decade also affects resolution. For the responses of the generic models, a value of 8 points per decade was chosen, which is around that produced by most commercial MT systems. If the number of points per decade is increased, then resolution increases. For typical high quality MT data, with a noise level of 2%, 8 points per decade of the Archean model results in 10.1 effective degrees of freedom of the 11 parameters. For 12 points per decade, this increases to 10.29, and for 16 points/decade to 10.30, whereas it reduces to 9.84 for 4 points/decade.

3.5. CSEM techniques

Controlled-source EM methods offer far higher resolving power in the intermediate field. With reasonable knowledge of the likely conductivity structure, CSEM surveys can be designed to optimally image the target (Maurer and Boerner, 1998; Maurer et al., 2000, 2010). When the receivers are in the near-field of the source, then only the source is seen in the phase response and no information can be obtained about the Earth's resistivity structure from the phase response alone (e.g., Boerner and West, 1989b; Boerner et al., 1993). Also, there is no advantage over MT if the receivers are in the far field of the transmitter, as then the source is a plane wave. The distance of concern is an inductive scale length, so is a function

Table 2
SVD eigenparameter analyses of the Archean model for low noise levels (1%): degrees of freedom = 10.5.

	Upper crust		Lower crust		Upper lithospheric mantle				Lower lithospheric mantle		Asthenosphere	Eigen parameter	Error
SV	ρ	h	ρ_2	h_2	ρ_3	h_3	ρ_4	h_4	ρ_5	h_5	ρ_6		
1	−52	−56	−38	−01	−04	−34	−11	−34	−06	−16	−01	$\rho_1 h_1$ (R_1)	0.0026
2	48	10	24	−29	01	−40	−09	−59	−11	−29	−02	$\sigma_1 h_4$	0.0030
3	−66	24	60	−27	08	12	09	−16	−03	−11	−01	$\sigma_1 \rho_2$	0.0042
4	12	−21	−07	14	08	54	46	−18	04	−61	−06	$h_3 h_5$	0.0064
5	−20	70	−36	33	−12	−25	01	−02	08	−39	−04	h	0.0075
6	04	−21	20	−20	−03	−23	−26	57	38	−53	−08	$h_4 h_5$	0.010
7	−01	07	−11	−03	13	32	−44	−37	70	13	−14	ρ_5	0.034
8	01	−13	28	33	−23	−36	53	−09	48	22	−20	$\rho_4 \rho_5$	0.053
9	−02	15	−40	−68	15	−08	41	10	12	12	−35	h_2	0.076
10	00	04	−11	−20	02	−07	22	−02	30	00	90	ρ_6	0.088
11	00	−01	05	−01	94	−23	06	05	02	01	01	ρ_3	0.50

of the period and the resistivity, and the greatest sensitivity is in between the near field and the far field (Boerner and West, 1989b).

For the three main source configurations, namely horizontal electric dipole (HED), vertical magnetic dipole (VMD, generated by a horizontal current loop), and horizontal magnetic dipole (HMD, generated by a vertical current loop), only HED or VMD needs to be considered for sensing the eMoho as it is impractical to build an HMD source that is large enough. Of an HED or VMD source, the most logistically practical for large-scale transmission is an HED source. Accordingly, we will consider the case of a grounded bipole source of 20 km in length centred on (0,0), with ground electrodes at (−10,0) and (10,0) and measurements off the end of the source bipole, i.e., along the positive x-direction, from (20,0) to (100,0) (all units in kilometres).

Here we consider the phases between the electric and magnetic fields; this avoids problems associated with "static shifts" that affect CSEM amplitude data in exactly the same manner as MT data (Jones, 1988). In CSEM, just as in MT, the phase and amplitude are related to each other through the Hilbert Transform (Qian and Boerner, 1992), so it is sufficient to examine phase alone. The phases of the in-line electric field (Ex) over the cross-line magnetic field (Hy), i.e., $\tan^{-1}$(Ex/Hy), for the 3 models at periods in the band 0.01 to 100 s and for sites from (20,0) to (100,0) are shown in Fig. 7. The phases of 0° (blue) occur when the receiver is in the near field of the source, and there is no point in making measurements at those frequency/position pairs. Near field source effects are well known in the CSEM method, and are well illustrated in, e.g., Boerner et al.'s (1993) CSAMT work in the Buchans mining camp, Newfoundland. Clearly, the differences between the models can be easily sensed.

For determining the sensitivity for each genetic model to the depth of the eMoho, the thickness of the lower crustal layer was varied such that the eMoho depth varied by ±20%, as for the DC and MT cases above. The phase differences between the −20% model and the +20% model are shown in Fig. 8 (note the differing contour scales between the three plots). A ±20% change in the eMoho depth introduces a maximum of ±3°, ±6°, and ±10° for the Archean, Proterozoic and Phanerozoic models respectively, with the maximum change being at the largest distance considered (100 km from the centre of the bipole).

Finally, testing for equivalency by halving the thickness and the resistivity of the lower crustal layer yields the phase differences shown in Fig. 9. The greatest sensitivity occurs obviously not in the source-dominated near-field, nor in the far-field, but in the intermediate field, as already discussed by Boerner and West (1989a, 1989b), amongst others.

4. Observations of the eMoho

Given the issues outlined above, it is not surprising that there have not been to date many substantiated reports of observations of the electric Moho. Below we review observations reported in the literature of a step-like change in resistivity that could be associated with the crust–mantle boundary.

4.1. DC resistivity results

Two large-scale DC resistivity experiments, one in southern Africa using the Cahora (formerly misspelt Cabora) Bassa DC powerline prior to service (Blohm et al., 1977) and the other in Australia using telephone lines taken out-of-service for a short time (Constable et al., 1984), were of a scale size that were possibly sufficient to image the eMoho.

The Cahora Bassa experiment, following on from prior work by van Zijl and Joubert (1975) in three locations in southern Africa, was reported as imaging a conducting lower crust, of some 50 Ω m,

Table 3
SVD eigenparameter analyses of the Proterozoic model for low noise levels (1%): degrees of freedom = 8.9.

	Upper crust		Lower crust		Upper lithospheric mantle				Lower lithospheric mantle		Asthenosphere	Eigen parameter	Error
SV	ρ	h	ρ_2	h_2	ρ_3	h_3	ρ_4	h_4	ρ_5	h_5	ρ_6		
1	−53	−62	−50	26	−01	−08	−02	−05	−01	−01	00	$\rho h \rho_2$	0.0024
2	78	−12	−50	35	−01	−06	−03	−02	−01	02	00	$\rho \sigma_2$	0.0029
3	−30	66	−31	48	−01	16	−03	26	02	23	03	h	0.0034
4	11	−36	16	−03	01	54	05	61	06	40	05	$h_3 h_4$	0.0044
5	−01	04	−12	01	02	37	23	20	34	−78	−18	h_5	0.019
6	02	−16	60	73	−03	−18	−10	03	11	−13	−07	$\rho_2 h_2$ (R_2)	0.037
7	00	01	−05	−09	−01	−13	−16	07	16	20	−94	ρ_6	0.078
8	00	−02	08	18	05	39	49	−34	−61	03	−28	ρ_5	0.13
9	00	00	−02	−06	−07	−29	−19	57	−67	−32	−06	$h_4 \sigma_5$	0.40
10	00	00	01	02	17	48	−79	−26	−16	−14	−01	ρ_4	>1.00
11	00	00	00	01	−98	14	−09	−10	−01	−01	00	ρ_3	

Table 4
SVD eigenparameter analyses of the Phanerozoic model for low noise levels (1%): degrees of freedom = 6.7.

	Upper crust		Lower crust		Upper lithospheric mantle		Lower lithospheric mantle		Asthenosphere	Eigen parameter	Error
SV	ρ	h	ρ_2	h_2	ρ_3	h_3	ρ_4	h_4	ρ_5		
1	−95	−27	−12	05	00	−02	00	−01	00	ρ	0.0020
2	30	−79	−48	20	00	−08	−01	−04	−01	h	0.0025
3	−04	51	−62	59	−01	02	−01	04	04	$h\sigma_2 h_2$ ($h_1 S_2$)	0.0039
4	01	−13	12	16	01	79	02	53	18	$h_3 h_4$	0.0055
5	−01	14	−58	−72	02	25	05	09	−22	$\rho_2 h_2$ (R_2)	0.033
6	00	−03	13	22	00	11	02	05	−96	ρ_5	0.047
7	00	00	−02	−07	−13	−42	−56	69	−05	$\sigma_4 h_4$ (S_4)	0.46
8	00	00	00	−01	−32	−29	80	41	00	ρ_4	>1.00
9	00	00	00	01	94	−17	19	23	00	ρ_3	

beneath the Kaapvaal Craton with a subsequent increase at a depth that could be associated with the crust–mantle boundary. Subsequent extensive MT measurements on the Kaapvaal Craton in 2003–2005, as part of the Southern African MagnetoTelluric Experiment (SAMTEX, Jones et al., 2009b), showed that the crust is resistive throughout its whole extent, apart from the enigmatic Bushveld Complex, and is nowhere below 300 Ω m (Evans et al., 2011). Hence, the Cahora Bassa DC responses are distorted by 3D effects, and cannot be interpreted in a 1D manner. This is a general problem for large-scale DC measurements.

The Australian experiment had potential electrodes up to 200 km apart, so the last one or two data points should sense the mantle, but the evidence in the data of a change at the crust–mantle boundary is non-existent.

4.2. MT results

Some MT practitioners have reported not finding conclusive evidence in their data of a step-like change in resistivity at depths that can be associated with the crust–mantle boundary (e.g., Chen et al., 1998; Gokarn et al., 1992; Jones, 1982), and most MT models of the lithospheric crust and mantle do not have a boundary at Moho depths. None of these studies will be reviewed here, as the reasons for the lack of evidence of an eMoho lies most likely primarily in the lack of resolution of the top of a layer of higher resistivity, as discussed above, rather than the lack of an eMoho sensu stricto. However, over the last decade some MT studies, particularly on cratons, have reported a resistivity step change at a depth that is close to the seismically-defined crust–mantle boundary. The first of these was Jones and Ferguson (2001) on the Slave Craton, northern Canada, and below we re-examine in detail the MT data from a site in the middle of the MT profile using more sophisticated modelling and statistical tools.

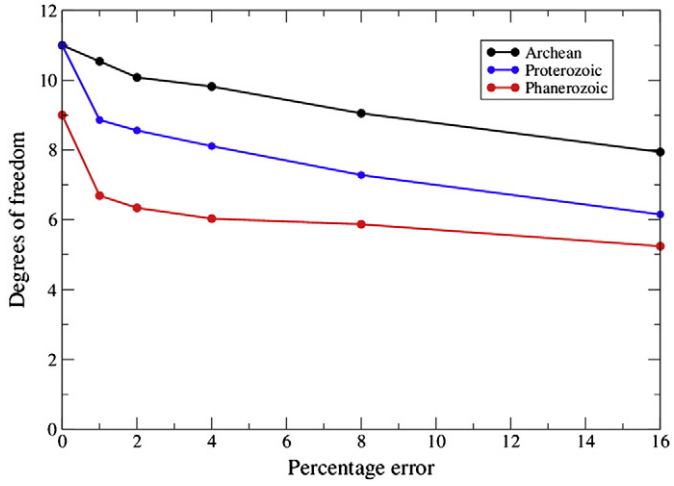

Fig. 6. Variation of degrees of freedom from SVD analyses with increasing noise levels (% added to impedance) for the three models of Fig. 1.

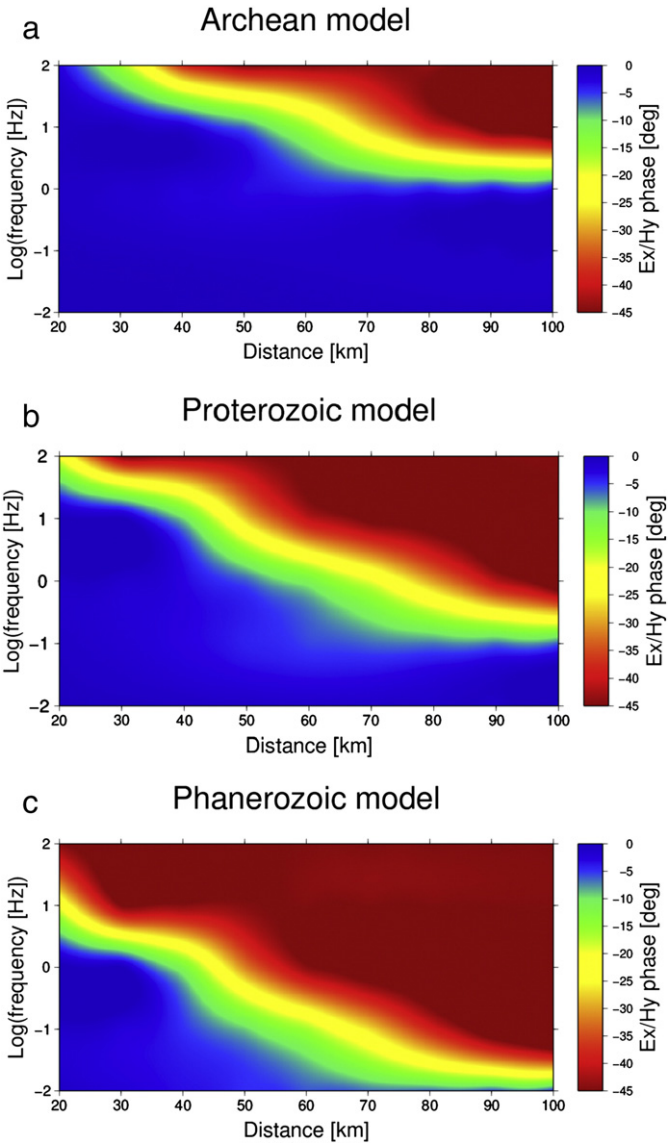

Fig. 7. CSEM impedance phases, given by Ex/Hy, at sites off the end of a bipole for (a) the Archean model, (b), the Proterozoic model, and (c) the Phanerozoic model. The phases of 0° (blue) occur when the receiver is in the near field of the source.

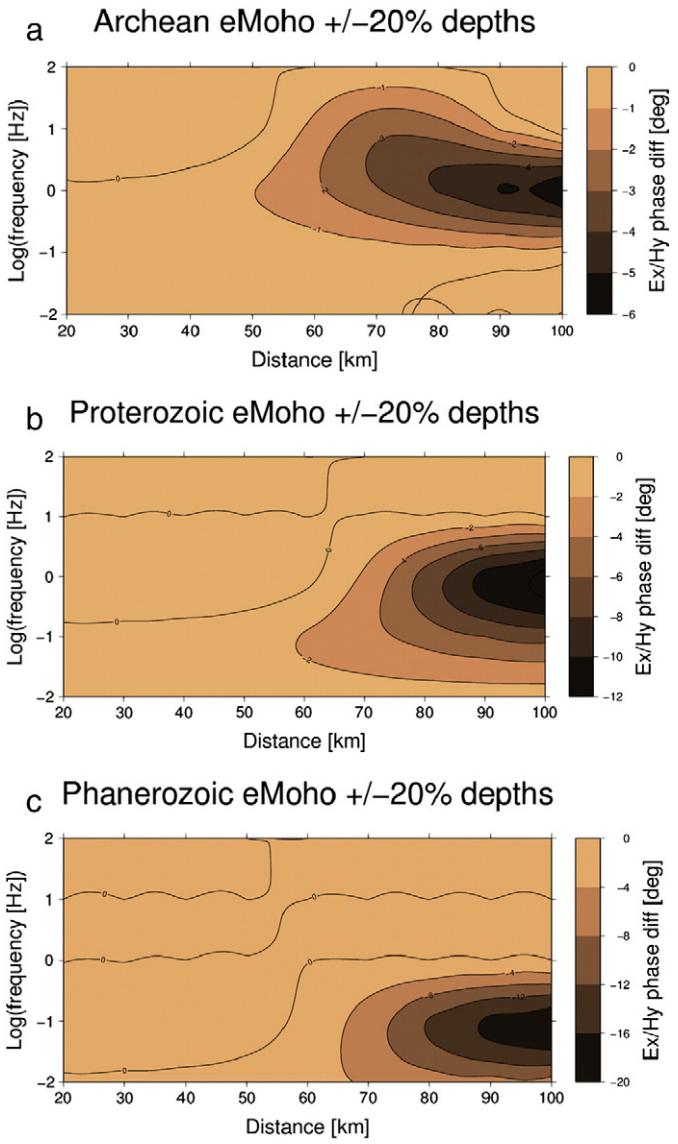

Fig. 8. CSEM Ex/Hy impedance phase differences between a model with the eMoho reduced by 20% and increased by 20% for (a) the Archean model, (b), the Proterozoic model, and (c) the Phanerozoic model. (Note the different contour scales between the three plots.) The phase differences of 0° mean that the eMoho variation cannot be sensed.

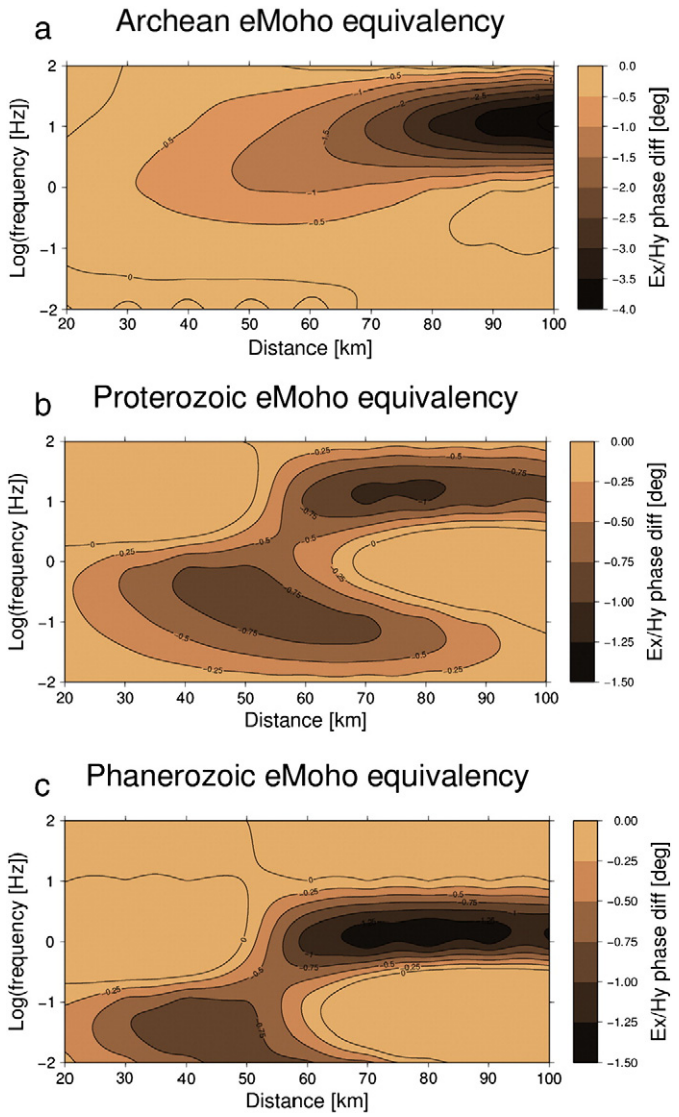

Fig. 9. CSEM Ex/Hy impedance phase differences between the original model and a model of the same conductance in the lower crust but half the thickness and resistivity for (a) the Archean model, (b), the Proterozoic model, and (c) the Phanerozoic model. (Note the different contour scales between the three plots.) The phase differences of 0° mean that the models are equivalent.

4.2.1. Slave Craton site sno106

Revisiting the Slave Craton data, Fig. 10 shows the original MT responses from the broadband (BBMT, Phoenix V5 system) and long period (LMT, GSC LiMS system) MT responses for site *sno106* in geographic coordinates. This site is in the middle of a 100-km-long profile, of 7 MT sites, between Yellowknife and Rae–Edso along the north shore of the arm of Great Slave Lake (see Fig. 1 in Jones and Ferguson, 2001). The profile lies within the formerly-named Anton Terrane or Anton Complex, now known to be the southern part of the regionally extensive Central Slave Basement Complex (Bleeker et al., 1999a, 1999b), which is the oldest part of the Archean Slave Craton. All sites along the profile display very 1D responses (see Fig. 2 in Jones and Ferguson, 2001), and site *sno106* was chosen as it has the best signal-to-noise ratio and thereby the highest quality data.

These BBMT and LMT responses were merged by:

1) Correcting each of them for local galvanic distortion using a Groom–Bailey like approach (Groom and Bailey, 1989; Jones, 2012a) similar to that of Jones (2012b) for an anisotropic 1D Earth, but assuming that the Earth is isotropic. Local distortion was small, with a twist of −5°, a shear of 11° (V5) and 19° (LiMS), and distortion anisotropy close to zero. Such low distortion in and of itself is unusual for MT data recorded on exposed Archean cratons, which generally exhibit high distortion due to near-surface inhomogeneities.
2) Merging the data together, taking the BBMT data at periods <100 s, and the LMT data at periods >100 s. This utilizes the highest quality data from the two systems.
3) Culling data outside the period band of 0.01–100 s. The shorter period data (<0.01 s) are not of interest as they relate to the uppermost crust, nor are the longer period data (>100 s), as the depth of penetration at 100 s is in excess of 100 km.

Then smoothed responses were derived by:

4) Undertaking a Rho + analysis (Parker and Booker, 1996) to identify and correct for outliers and inconsistencies between the apparent resistivity and the phase responses.

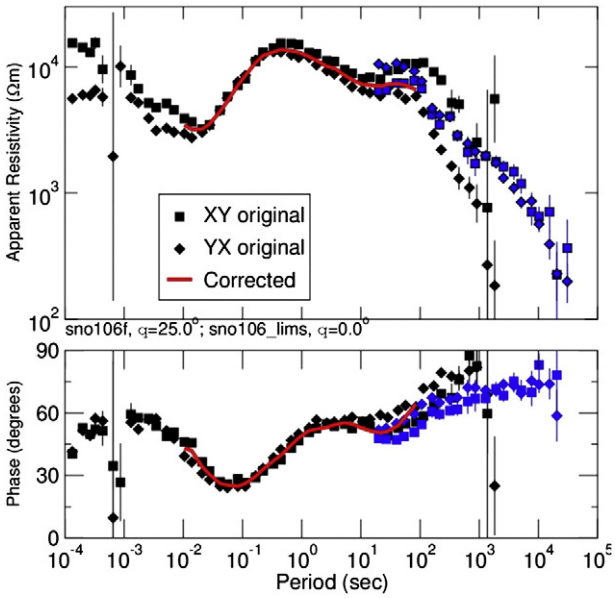

Fig. 10. Original MT responses from site *sno106* (BBMT: black symbols, LMT: blue symbols) and corrected 1D responses (red lines).

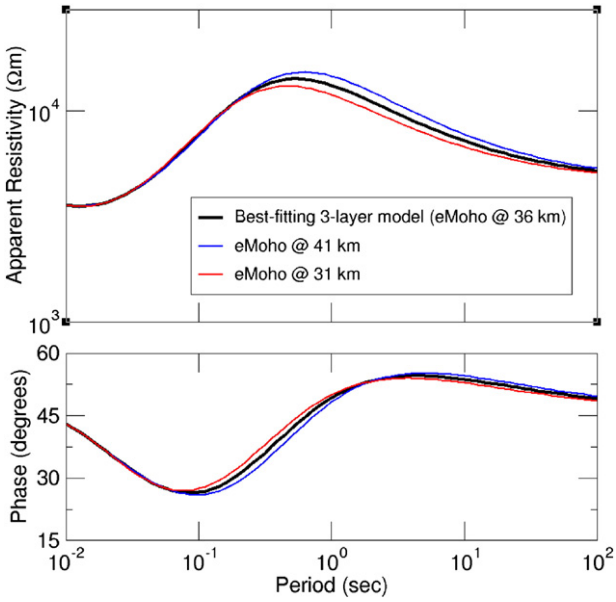

Fig. 11. Result of varying depths to the eMoho for the southern Slave Craton, from 36 km, by ±14% (31–41 km).

The smoothed data are also shown in Fig. 10. These smoothed data are modelled for minimum structure using both a minimum number of uniform resistivity layers approach and an overdetermined least-gradient approach. The former was accomplished with the MINIM algorithm of Fischer and Le Quang (1981), and the latter with the updated 1D OCCAM algorithm of Constable et al. (1987). Through trial-and-error, it was determined that the data could be explained sufficiently by 4 layers, each of uniform, isotropic resistivity; any fewer led to high misfit, and any more did not statistically reduce the level of misfit. The best-fitting 4-layer model that could be found is listed in Table 5, together with a sensitivity analysis conducted using SVD of the model parameters.

The southwestern part of the Slave Craton is highly unusual in that the bulk of the crust below some 5 km to approximately 35 km is extremely resistive (>40,000 Ω m). In addition, contrary to expectations from laboratory considerations (see above), the upper lithospheric mantle is moderately resistive (~4000 Ω m); this is discussed further below. This means that the problem is one of resolving the top of a "conductor" beneath an extensive resistive region, which is a different scenario from that discussed for the three generic models where the problem there is one of resolving the base of a conductor/top of a resistor. To determine at which periods the MT data are sensing the eMoho for this resistivity-depth distribution, the same exercise was performed as for Fig. 4 with varying the eMoho depth by ±5 km (±14%, Fig. 11) in this case. Sensitivity to the eMoho depth is greatest in the apparent resistivity data at around 1 s, where sensitivity to the different models is a minimum in the phase data. To determine how well the eMoho depth is defined by the model, the data misfits have to be considered not globally overall periods of 0.01–100 s, but in the band 0.1–0.3 s for phase and 0.3–10 s for apparent resistivity. This is to ensure that the average misfit is not misleading due to overfitting data of little interest, and poorly fitting data of most interest (for a discussion of this problem see, e.g., Jones, 1993). Reducing the period band of interest to 0.1–10 s reduces the number of layers required to three and the penetration depths, estimated by the real part of Schmucker's C function, to 4.6–81 km.

Having established that a three-layer model is sufficient for the smoothed data in the range of 0.1–10 s, we return to the original, unsmoothed but distortion-corrected BBMT data and investigate individual misfits for best-fitting layered-Earth and continuous models (Fig. 12). The minimum possible RMS, given by Parker's (1980) D+, for these data without an error floor being assigned is 7.5, indicative of error estimates that are overly optimistic and are far too small. This is a known problem with parametric estimates of error, particularly when the number of samples in the estimates becomes large. Chave and Jones (1997) demonstrated that error estimates calculated by

Table 5
Parameters of best-fitting 4-layer model to smoothed, distortion-corrected data in the band 0.01 s to 100 s from site *sno106*.

Layer	Resistivity (Ω m)	Error (Ω m)	Thickness (km)	Error (km)	Depth (km)	Error (m)
1	3810	3750–3880	4.49	4.27–4.73	4.49	4.27–4.73
2	84,100	57,900–122,000	27.5	26.5–28.6	32.0	30.8–33.3
3	4840	4750–4940	276	265–283	308	296–316
4	28	8.69–88.6	–	–	–	–

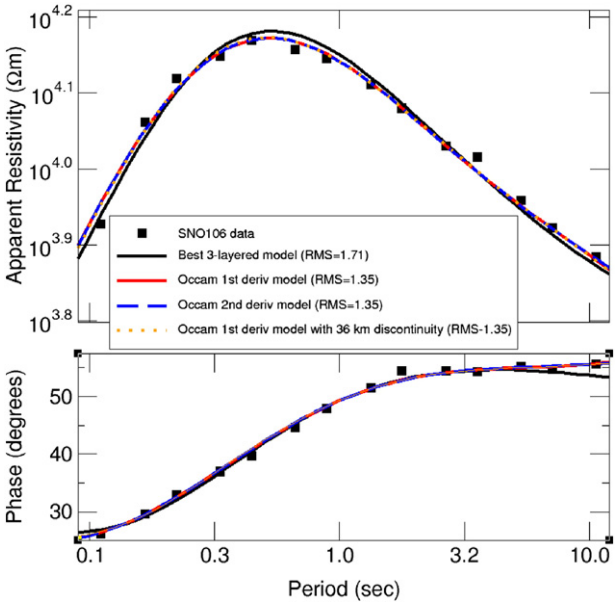

Fig. 12. MT observations in the period band 0.1 to 10 s together with the theoretical responses of the three best-fitting models shown in Fig. 1, the 3-layer model (black lines) and the Occam models (1st (red lines) and 2nd (blue lines) derivative and 1st derivative with permitted 36 km discontinuity).

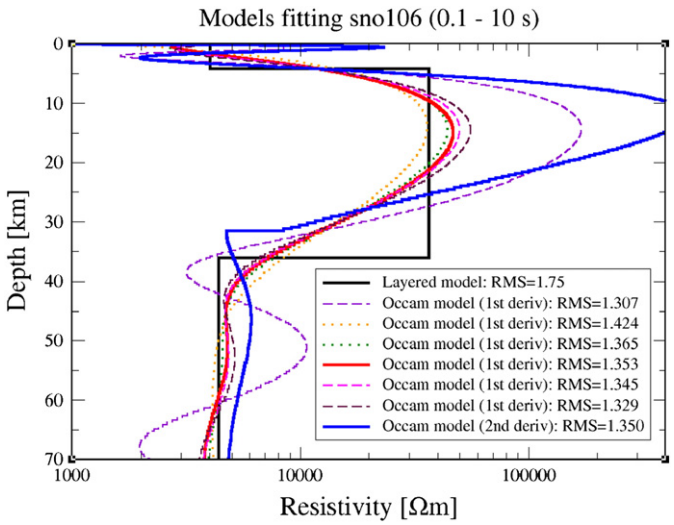

Fig. 13. Models fitting the corrected 1D MT responses shown in Fig. 10 (red lines). Black line: 3-layered Earth. Other lines are a family of continuous Occam least-structure models minimizing first derivative of conductivity with depth for varying target misfits. Red solid line: preferred model with misfit of RMS = 1.35. Blue solid line: least structure continuous model minimizing second derivative of conductivity with depth with RMS = 1.35.

Phoenix's processing code are some 3–5 times too small compared to robust, jackknife-derived error estimates at periods of around 1 s. To counter such issues, an error floor is assigned: errors that are above the error floor are unchanged, whereas those below the error floor are increased to the error floor value. Assigning an error floor of 1% in impedance, which is approximately 2% in apparent resistivity and 0.58° in phase, yields a reasonable minimum possible RMS of 1.13.

The best-fitting 3-layer model to these data, found using MINIM, has an RMS of 1.71 and is given in Table 5 and is shown in Fig. 13 (black line). Although the overall fit is reasonable in a global misfit sense, problems with considering only RMS were emphasized in Jones (1993). Higher order measures of fit need to be employed to test the randomness of the residuals. The individual residuals between the observed and modelled data exhibit serial correlations, with unacceptable Durbin–Watson (Durbin and Watson, 1950; Durbin and Watson, 1951) statistics of 0.18 for apparent resistivity and 0.14 for phase, whereas the expectation value for randomly distributed residuals is 2. The Durbin–Watson statistic is one of a family of higher-order measures of fit beyond characterizing the distance between data and the model responses solely by the RMS. Another robust measure of the "colour" of the fit is the Spearman statistic used by Smith and Booker (1988) to test the significance of a trend.

SVD analysis of the 3-layer model shows that of the 5 model parameters, 4 are well-resolved and one is marginally resolved (4.8 degrees of freedom), that one being the resistivity of the second layer times the thickness of the first layer (Table 7).

The depth to the base of the second layer ($d_2 = h_1 + h_2$) is determined from combining all of the eigenparameters that, taken together, give h_1 and h_2. The errors on the model parameters, derived by the linearized SVD analysis, are given in Table 6, and d_2 is derived as 36.1 ± 5 km. If we fix the eMoho depths to those extremal values, and search for the other model parameters, then the best-fitting models found have misfits that are 2.29 and 2.30 for 31 km and 41 km eMohos respectively, both significantly greater than the RMS of 1.71 achieved by the model with an eMoho at 36 km. This demonstrates the highly non-linear nature of EM methods, and that linearized appraisal must be treated with caution (see, e.g., Ledo et al., 2004). Varying the depths to the eMoho from 31 km to 41 km yields the RMS misfits shown in Fig. 14 and listed in Table 8, where a sharp minimum is observed centred on an eMoho depth of 36.5 km with a width of around ± 1 km to remain below an RMS of 1.75.

Table 6
Parameters of best-fitting 3-layer model to distortion-corrected data in the band 0.1 s to 10 s from site *sno106*.

Layer	Resistivity (Ω m)	Error (Ω m)	Thickness (km)	Error (km)	Depth (km)	Error (m)
1	4030	2700–6000	4.22	4.15–4.63	4.22	4.265–4.730
2	36,600	18,000–73,000	31.9	27.0–38.1	36.1	31.2–42.7
3	4390	4150–4630	–	–	–	–

Table 7
SVD analysis of the data from *sno106* and the model of Table 5. Degrees of freedom = 4.8.

	Uppermost crust		Crust		Lithospheric mantle	Eigenparameter	Error
Singular value	ρ	h	ρ_2	h_2	ρ_3		
1	−71	57	−24	−26	−06	σh (S_1)	0.0040
2	18	−22	06	−81	−50	h_2	0.0068
3	−10	06	15	06	−86	ρ_3	0.021
4	54	44	−71	11	−09	$\rho\rho_2$	0.099
5	35	66	64	−17	03	$h\rho_2$	0.61

Fitting first-derivative least-structure Occam models to these data yields a family of models with varying misfits, from an RMS of 1.31 to 1.42 (Fig. 13). Those with the smallest misfit exhibit oscillatory behaviour (dashed lines in Fig. 13) whereas those with higher misfit are overly smooth (dotted lines, Fig. 13). The optimum misfit level is judged to be that at which the oscillatory behaviour is just becoming manifest, which occurs at an RMS = 1.35. This value is some 22% greater than the absolute minimum possible, given by the D+ solution of 1.11. Also shown in Fig. 13 (dashed purple line) is the Occam model minimizing the second derivative of conductivity with depth. The rapid decrease in resistivity below 20 km to a uniform value of the order of 4000–5000 Ω m at a depth of around 35 km is clearly evident in all smooth models.

Permitting a step-like discontinuity in the continuous model, with the locations of the step varying from 31 km to 41 km, yields the families of models shown in Fig. 15 for both 1st derivative smoothing (Fig. 15a) and 2nd derivative smoothing (Fig. 15b) minimization, all fitting to an RMS of 1.35. Particularly the 2nd derivative smoothing strongly suggests that the upper lithospheric mantle is of uniform

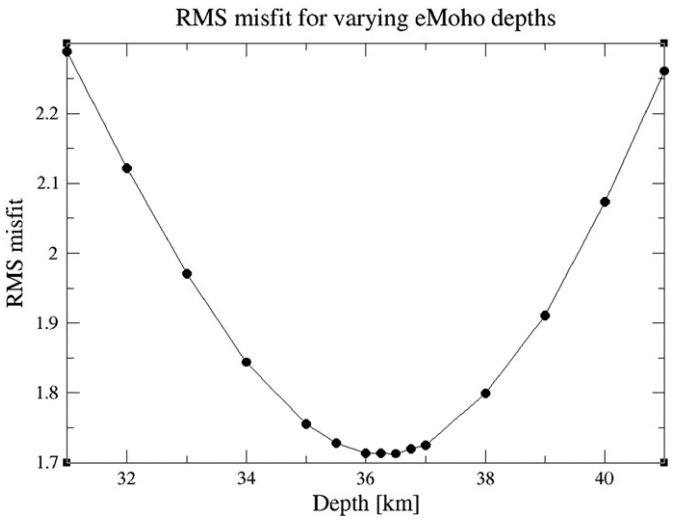

Fig. 14. RMS misfits for best-fitting 3-layered models with the discontinuity between the 2nd (crustal) and 3rd (mantle) layers at a fixed depth.

Table 8
RMS misfit for 3-layer model and Durbin–Watson statistics for the 1st (1) and 2nd (2) derivative Occam models with a permitted discontinuity at varying depths from 31 km to 41 km.

Depth of discontinuity	31 km	32 km	33 km	34 km	35 km	36 km	37 km	38 km	39 km	40 km	41 km
Layered RMS	2.29	2.12	1.97	1.84	1.76	1.71	1.73	1.80	1.91	2.07	2.30
Occam1 DW rho	0.31	0.30	0.30	0.31	0.33	0.36	0.40	0.42	0.48	0.46	0.44
Occam1 DW pha	0.98	0.96	0.98	1.01	1.09	1.16	1.29	1.39	1.47	1.47	1.40
Occam2 DW rho	0.27	0.40	0.43	0.43	0.46	0.49	0.53	0.52	0.47	0.47	0.46
Occam2 DW pha	0.83	0.98	1.02	1.06	1.15	1.18	1.23	1.29	1.26	1.26	1.22

resistivity with a value of the order of 4500 Ω m. With the permitted discontinuity at 36 km, the smooth model has fewer oscillations than the greater depths, and also has superior Durbin–Watson statistics than for the shallower depths (see Table 8).

Taken together, the conclusion of all of these model studies is that the eMoho beneath site *sno106* is at a depth of 35–37 km. This value correlates well with seismic estimates of the Moho beneath the "Anton Terrane" between Yellowknife and Rae–Edso in the SW part of the Slave Craton. A seismic refraction experiment, the standard method of determining the seismic Moho, along the profile from Rae–Edso to Yellowknife gave a flat Moho of around 33 (32–35) km (Fernandez Viejo and Clowes, 2001) with a strong contrast in velocity on either side of it, from 6.9 km/s to 8.2–8.3 km/s. A reflection profile along the same traverse as the refraction and MT profiles shows a remarkably flat Moho at 11 s to 12 s TWTT, which converts to 33–35 km in depth

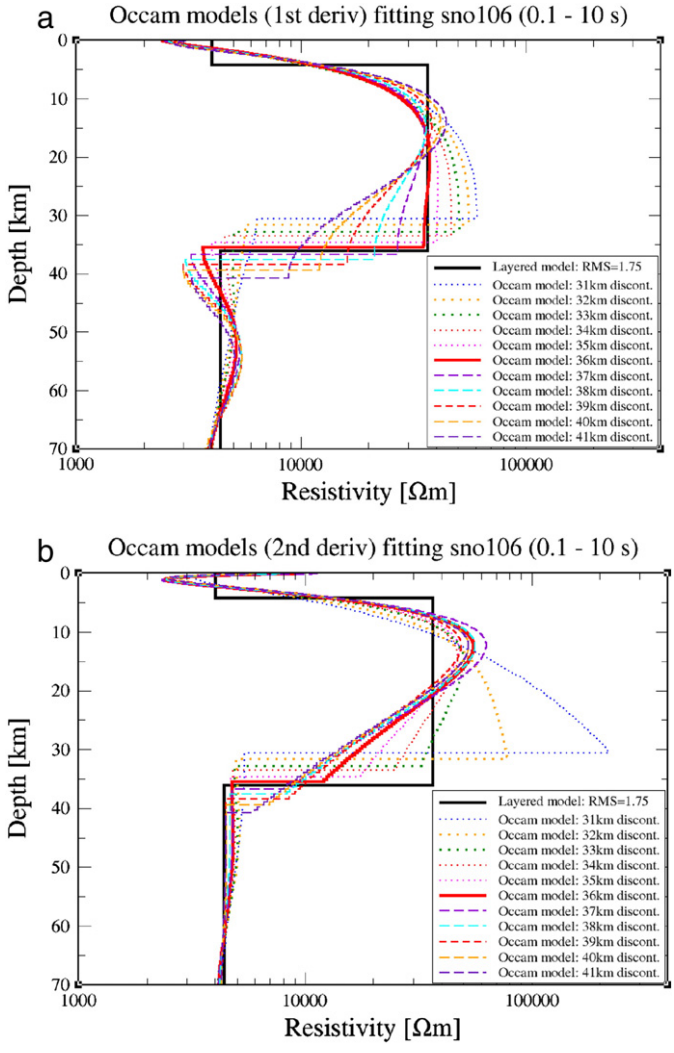

Fig. 15. Families of Occam models allowing a discontinuity at varying depths from 31 km to 41 km. (a) First derivative models. (b) Second derivative models.

(Cook et al., 1999). Finally, analysis of the teleseismic data recorded over many years at the Yellowknife array by Bostock (1998) yielded a Moho depth beneath the array, which is centred some 30 km to the east of site *sno106*, of 36.5 km.

These four estimates, 32–35 km (refraction), 33–35 km (reflection), 36.5 km (teleseismic) and 36 km (MT) can all be reconciled by assuming that the crustal velocity function used for converting the teleseismic RF times to depths needs to be up to 6% faster, and that there is a residual site gain static shift on the electric fields of the MT responses of up to 3%. These would yield a Moho in the range of 34–35 km.

Although the cause of the low resistivity in the uppermost mantle observed beneath the southern part of the Slave Craton is peripheral to this paper, it is worthwhile to note that none of the current explanations for reducing resistivity in mantle minerals are valid to explain this observation. The mantle directly below the Moho is known to be cold, around 450 °C, and to be ultra-depleted in iron, based on xenoliths from the Drybones Bay kimberlite just to the east of Yellowknife (Carbno and Canil, 2002). Dry olivine under these conditions (Mg# = 93.0) would have a resistivity of the order of 10^8 Ω m (Fullea et al., 2011; Jones et al., 2009a). Temperature would have to be 1000 °C to explain the observed value of 4000 Ω m. Water, or more correctly hydrogen diffusion, will reduce the resistivity significantly, but unacceptably high values of greater than 2000 wt ppm water in olivine are required to reduce the resistivity to 4000 Ω m (Jones et al., 2012), whereas values of the order of 50–100 wt ppm are found in xenolith samples from cratonic lithospheric mantle (Baptiste et al., 2012; Peslier et al., 2010). If the water content is high, up to 200 wt ppm, then a sub-Moho temperature of 600 °C is sufficient to yield the resistivity observed, but even this temperature is far too high and unreasonable. Other speculations to explain the low resistivity in the lithospheric mantle include carbon (Duba and Shankland, 1982), sulphides (Ducea and Park, 2000), and mineral grain size consideration (ten Grotenhuis et al., 2004), but none of these have supporting evidence or are without serious objection.

4.2.2. Other MT observations of the eMoho

Similar to the Slave Craton case, an eMoho is reported for the East Indian (alternatively called the Singhbhum or Singhbhum-Orissa) Craton (Bhattacharya and Shalivahan, 2002a, 2002b; Shalivahan and Bhattacharya, 2002), where the crust is also found to be highly resistive (30,000 Ω m) and the upper mantle moderately resistive (8500 Ω m). In that work 2D inversion was applied but no sensitivity analysis was conducted. An eMoho was modelled at a depth of 46 ± 2 km. There are no comparable seismic studies with which to correlate that depth with, but that eMoho exceeds significantly the depth to the seismically-defined crust–mantle boundary based on receiver functions for other Precambrian regions in India (Jagadeesh and Rai, 2008).

MT studies on the eastern part of the North China Craton reveal a strong gradient zone in electrical resistivity that is compatible with the seismic Moho (Wei et al., 2008). At most locations, the gradient zone is related to a thin, low resistivity layer presumed to lie at the base of the crust.

In two other Precambrian regions of Canada there is the inference of an eMoho. One of these is across the Snowbird Tectonic Zone (STZ) separating the Rae and Hearne domains of the composite Western Churchill Craton lying west of Hudson's Bay in Nunavut, northern

Canada. A collocated teleseismic and MT profile was undertaken in 1998 along a 350-km-long transect straddling the STZ. From receiver function analyses, the Hearne domain exhibits a seismically more complex (multi-layered) crust of 41–42 km in thickness, compared to a seismically simpler crust of 39 km thickness for the Rae domain (Jones et al., 2002). These seismic observations were substantiated in a more recent study (Thompson et al., 2010). In its electrical response, the crust of the Rae north of the Snowbird Tectonic Zone exhibits very low total integrated conductance, below 1 Siemen, similar to the Slave and Singhbhum cratons (Jones et al., 2002). In contrast to those two localities though, the Rae mantle lithosphere is highly resistive, in excess of 65,000 Ω m. For the Hearne domain there is a more structured crust, with a conducting lower crust (some hundreds of Ω m) above a moderately resistive mantle (some thousands of Ω m). 2D modelling of the MT data, whilst not exacting, does infer for both regions a strong increase in resistivity at depths that are comparable to the Moho (see Fig. 3 in Jones et al., 2002).

Finally for Canada, a 300-km-long MT transect of 20 sites from the Slave Craton to the Bear Province to the west yielded models with sharp discontinuities for some locations at likely depths for the crust–mantle boundary (Spratt et al., 2009). Focussed 2D modelling of sites on the Mackenzie Platform, west of the Great Bear Magmatic Zone, reveals a highly resistive crust (>30,000 Ω m) overlying a more conducting upper mantle (~5000 Ω m), with a sharp transition between the two at around 28–30 km (see Fig. 9 in Spratt et al., 2009).

In other parts of the globe, comparing the seismic Moho depths for the Baltic Shield with maps of maxima in resistivity, Plotkin et al. (2011) show a prominent correlation in the regions of maximum Moho deepening down to 60–65 km near the Ladoga–Bothnia zone (east–central Finland), to approximately 40 km in the region of the Vyborg Rapakivi granite rock massif, and to 56 km near the western coast of the Gulf of Bothnia. Whilst these are not correlations in depth, they do speak of lateral crustal resistivity variation being related to Moho variation.

4.2.3. Joint teleseismic and MT inversion approaches

Formal joint inversions of teleseismic and MT data together result in models that have a step-like change at the Moho, given that the Moho is such a dominant seismic feature. These studies were initiated by Moorkamp et al. (2007), who used a genetic algorithm (GA) stochastic modelling approach to find consistent models that fit both P receiver functions (pRF) and MT responses simultaneously. The tie between the two models was the interface positions; there was no physical property relationship defined, as is undertaken in joint inversions using, for example, cross gradients (Gallardo and Meju, 2003, 2004). Teleseismic and MT data were taken from a site in the centre of the Slave Craton, and joint inversion yielded models with a compatible Moho and eMoho at 35 km depth (with an assumed crustal velocity profile to convert RFs from time to depth).

Subsequently, Moorkamp and colleagues included simultaneously fitting surface wave dispersion curves (SW) at the same time as pRF and MT (Moorkamp et al., 2010). The advantage of this is that the crustal velocity profile does not need to be assumed, but is derived simultaneously. Applying the SW + pRF + MT approach to the central Slave site used previously, the Moho and the eMoho were identified at a deeper depth of 39 km, the difference being that the assumed crustal velocity in the prior inversions of 3.4 km/s was too slow, whereas the SW dispersion curve required a crustal velocity of 3.8 km/s. The revised depth is consistent with pRF studies of sites located in the central Slave Craton (Bank et al., 2000). Applying the joint inversion to sites on the Kaapvaal Craton yielded mutually-consistent models with the Moho/eMoho at a depth of 37 km, in agreement with prior studies (see Moorkamp et al., 2010 for details).

Roux and colleagues extended the approach to consider anisotropic layering (Roux et al., 2008), jointly inverting anisotropic SW dispersion curves and anisotropic 1D MT data. The technique was applied to sites in northern Germany, and a Moho thickness of 35 km was determined, consistent with prior information. The MT response was unusual in that the lower crust was modelled as electrically isotropic, whereas the upper lithospheric mantle was modelled as significantly anisotropic. Thus, the eMoho is characterized in this location more by the change in anisotropy properties than by a change in actual resistivity.

4.3. CSEM results

There have been very few large-scale CSEM experiments designed to penetrate to the mantle. The most extensive investigations globally have occurred in northern Finland/NW Russia, as a consequence of studies involving the Khibiny magneto-hydrodynamic (MHD) generator source plus other sources. The Khibiny source was unique, and comprised a 7 km bipole grounded into the sea on either side of a peninsula off the Kola Peninsula in northwestern Russia generating 80 MW of power (Velikhov et al., 1986). In addition, an experiment was constructed that made use of power transmission lines (Zhamaletdinov et al., 2009). All of the CSEM results are reviewed by Zhamaletdinov (2011) and Zhamaletdinov et al. (2011), and a spatially averaged eMoho is identified for the northern Baltic Shield at a depth of 35–45 km (Zhamaletdinov, 2011). Interestingly, the eMoho is associated again with a reduction in resistivity, from >100,000 Ω m to ~50,000 Ω m.

5. Conclusions and recommendations

Laboratory studies suggest that there should be a step-like change in electrical conductivity at the continental crust–mantle boundary, an electric Moho (eMoho). However, imaging and observing the eMoho using electrical or electromagnetic methods are not trivial tasks. The identification of an eMoho has been elusive, appearing, when it does, serendipitous and occasionally capricious.

In most locations on Earth there exists a lower crustal layer that is more conducting than the upper crust and the upper lithospheric mantle. The parameters of this resistive–conductive–resistive sandwich, called H-type in DC resistivity, are notoriously difficult to resolve due to equivalency of models with the same vertically-integrated conductance (conductivity-thickness product). In a very few regions however, all of them Archean in age, the lower crust is more resistive than the upper mantle, meaning that the target is the depth to the top of a relative “conductor”, which is far easier than resolving the depth to the top of a resistor.

For DC methods, equivalency is a severe problem, as shown in Fig. 3. Only at electrode separation distances of greater than 3 times the depth to the Moho can the equivalent models be distinguished, and only then with virtually perfect data for an Earth that is laterally uniform without 3D effects and undulations in the Moho. If lower crustal resistivity is known however, then resolution of the depth of the eMoho can be determined at electrode separations of the order of 1.5 times its depth (Fig. 2).

Magnetotelluric and controlled-source EM methods fare somewhat better in their resolution and equivalency properties, and the latter can be designed to optimally image the eMoho. MT has the logistical and expense advantage that no large source is required, but the disadvantage on PreCambrian regions being that the greatest sensitivity to the eMoho depth occurs in the MT “dead-band” between 0.1 and 10 s (Fig. 4). This means that great care has to be taken with site installation, and multiple nights of recording are required. For Phanerozoic regions, given the higher conductance of the lower crust the sensitivity is in the 10 s–200 s band (Fig. 4), for which there is usually strong signals, particularly Pc3 and Pc4 continuous pulsations (McPherron, 2005). For all regions however, very high quality data are required; as data quality decreases so does the number of eigenparameters resolved (Fig. 6),

and the first to become unresolved is the integrated resistivity of the lower crust.

For CSEM, logically the simplest source is a long grounded bipole, and the responses off the end of a 20 km bipole have been simulated (Fig. 7). Too close to the source however, where "close" is an inductive scale length given by the resistivity and the period, the receivers are in the near-field and in phase data the Earth response is overwhelmed by the source response (blue regions in Fig. 7). At distances too far, the far-field, then the source signal will be weak, and there is no advantage in using a controlled-source over natural-source MT. Particularly to address the equivalency problem, then measurements need to be made in the intermediate field (Fig. 9).

Field examples were discussed from the three methods, focussing primarily on MT results, and in particular on the data from a site in the southwestern part of the Slave Craton. Detailed analyses of the data from *sno106* showed that an eMoho at around 36 km is most consistent with the data, not only in an RMS misfit sense but also in terms of the statistics of the residuals using a Durbin–Watson test. That depth is, to within error, exactly that of the seismic Moho determined from teleseismic analysis, but it is somewhat deeper than the reflection and refraction Mohos at 33–35 km. These four estimates can all be made consistent by assuming that the crustal velocity function used for converting the teleseismic RF times to depths needs to be 6% faster, and that there is a residual site gain static shift on the electric fields of the MT responses of 3%.

Most of the other believable results on resolving an eMoho also come from situations like the southwestern Slave Craton, i.e., a highly resistive lower crust over a less resistive upper mantle.

Joint inversion approaches have their utility, but prior to their use it must be first established that there is a reasonable expectation of an eMoho from the MT data before the outcomes of joint inversions are acceptable.

EM methods have their utility in imaging structures within the Earth. Sensitivity to a small percentage of a minor interconnected phase, such as a saline fluid, melt, or conducting metasediments, increases the electrical conductivity by orders of magnitude. Imaging and observing an eMoho are though difficult tasks usually at the edge, and sometimes beyond, resolution, even with the highest quality data. Nonetheless, there are some localities for which an eMoho can be defined with confidence.

Acknowledgements

Forward calculations for the DC resistivity models were undertaken using the routine CALRES distributed as part of the VFSARES code by S.P. Sharma Sharma (2012), and the CSEM calculations were undertaken with a code provided by Doug Oldenburg and Roman Shekhtman (pers. comm., 2012). Steve Constable i thanked for providing the latest version of his Occam 1D code (Constable et al., 1987). Those four authors are thanked for making their codes freely available. The MT and SVD calculations were undertaken with codes written by the author. The author thanks the editor, Irina Artemieva, and the two reviewers for comments on the original version of this manuscript.

References

Bailey, R.C., 1970. Inversion of the geomagnetic induction problem. Proceedings of the Royal Society of London A315, 185–194.
Bank, C.G., Bostock, M.G., Ellis, R.M., Cassidy, J.F., 2000. A reconnaissance teleseismic study of the upper mantle and transition zone beneath the Archean Slave Craton in NW Canada. Tectonophysics 319 (3), 151–166.
Baptiste, V., Tommasi, A., Demouchy, S., 2012. Deformation and hydration of the lithospheric mantle beneath the Kaapvaal Craton, South Africa. Lithos 149, 31–50.
Bhattacharya, B.B., Shalivahan, 2002a. The electric Moho underneath Eastern Indian Craton. Geophysical Research Letters 29 (10).
Bhattacharya, B.B., Shalivahan, 2002b. Moho from magnetotelluric studies in Eastern Indian Craton and Slave Craton, Canada. Journal of the Geological Society of India 60 (6), 687–690.
Bleeker, W., Ketchum, J., Davis, W., 1999a. The Central Slave Basement Complex, part II: age and tectonic significance of high-strain zones along the basement-cover contact. Canadian Journal of Earth Sciences 36 (7), 1111–1130.
Bleeker, W., Ketchum, J., Jackson, V., Villeneuve, M., 1999b. The Central Slave Basement Complex, part I: its structural topology and autochthonous cover. Canadian Journal of Earth Sciences 36 (7), 1083–1109.
Blohm, E.K., Worzyk, P., Scriba, H., 1977. Geoelectrical deep soundings in Southern Africa using the Cabora Bassa power-line. Journal of Geophysics-Zeitschrift Fur Geophysik 43 (4), 665–679.
Boerner, D.E., West, G.F., 1989a. A generalized representation of the electromagnetic-fields in a layered Earth. Geophysical Journal-Oxford 97 (3), 529–547.
Boerner, D.E., West, G.F., 1989b. A spatial and spectral-analysis of the electromagnetic sensitivity in a layered Earth. Geophysical Journal International 98 (1), 11–21.
Boerner, D.E., Wright, J.A., Thurlow, J.G., Reed, L.E., 1993. Tensor CSAMT studies at the Buchans mine in central Newfoundland. Geophysics 58 (1), 12–19.
Bostock, M.G., 1998. Mantle stratigraphy and evolution of the Slave Province. Journal of Geophysical Research-Solid Earth 103 (B9), 21183–21200.
Carbno, G.B., Canil, D., 2002. Mantle structure beneath the SW Slave Craton, Canada: constraints from garnet geochemistry in the Drybones Bay kimberlite. Journal of Petrology 43 (1), 129–142.
Chave, A.D., Jones, A.G., 1997. Electric and magnetic field galvanic distortion decomposition of BC87 data. Journal of Geomagnetism and Geoelectricity 49 (6), 767–789.
Chen, C.S., Chen, C.C., Chou, K.S., 1998. Deep electrical structure of Taiwan as inferred from magnetotelluric observations. Terrestrial Atmospheric and Oceanic Sciences 9 (1), 51–68.
Constable, S., 2006. SEO3: a new model of olivine electrical conductivity. Geophysical Journal International 166 (1), 435–437.
Constable, S., McElhinny, M.W., McFadden, P.L., 1984. Deep Schlumberger sounding and the crustal resistivity structure of central Australia. Geophysical Journal of the Royal Astronomical Society 79 (3), 893–910.
Constable, S., Parker, R.L., Constable, C.G., 1987. Occam's inversion: a practical algorithm for generating smooth models from electromagnetic sounding data. Geophysics 52 (3), 289–300.
Cook, F.A., van der Velden, A.J., Hall, K.W., Roberts, B.J., 1999. Frozen subduction in Canada's Northwest Territories: lithoprobe deep lithospheric reflection profiling of the western Canadian Shield. Tectonics 18 (1), 1–24.
Cook, F.A., et al., 2010. How the crust meets the mantle: lithoprobe perspectives on the Mohorovii discontinuity and crust–mantle transition. Canadian Journal of Earth Sciences 47 (4), 315–351.
Duba, A.G., Shankland, T.J., 1982. Free carbon and electrical conductivity in the Earth's mantle. Geophysical Research Letters 9 (11), 1271–1274.
Ducea, M.N., Park, S.K., 2000. Enhanced mantle conductivity from sulfide minerals, southern Sierra Nevada, California. Geophysical Research Letters 27 (16), 2405–2408.
Durbin, J., Watson, G.S., 1950. Testing for serial correlation in least squares regression. 1. Biometrika 37 (3–4), 409–428.
Durbin, J., Watson, G.S., 1951. Testing for serial correlation in least squares regression. 2. Biometrika 38 (1–2), 159–178.
Eaton, D.W., 2006. Multi-genetic origin of the continental Moho: insights from Lithoprobe. Terra Nova 18 (1), 34–43.
Edwards, R.N., Bailey, R.C., Garland, G.D., 1980. Crustal and upper mantle conductivity studies with natural and artificial sources. In: Strangway, D.W. (Ed.), The Continental Crust and Its Mineral Deposits, J.T. Wilson Symposium, Special Publ. 20. Geol. Assoc. Canada, pp. 255–271.
Edwards, R.N., Bailey, R.C., Garland, G.D., 1981. Conductivity anomalies — lower crust or asthenosphere. Physics of the Earth and Planetary Interiors 25 (3), 263–272.
Evans, R.L., et al., 2011. The electrical lithosphere beneath the Kaapvaal Craton, Southern Africa. Journal of Geophysical Research — Solid Earth 16.
Fernandez Viejo, G., Clowes, R.M., 2001. Lithospheric structure beneath the Archaean Slave Province and ProterozoicWopmay orogen, northwestern Canada, from a Lithoprobe refraction/wide-angle reflection survey. Geophysical Journal International 153 (1), 1–19.
Fischer, G., Le Quang, B.V., 1981. Topography and minimization of the standard-deviation in one-dimensional magnetotelluric modeling. Geophysical Journal of the Royal Astronomical Society 67 (2), 279–292.
Frost, B.R., Fyfe, W.S., Tazaki, K., Chan, T., 1989. Grain-boundary graphite in rocks and implications for high electrical conductivity in the lower crust. Nature 340 (6229), 134–136.
Fullea, J., Muller, M.R., Jones, A.G., 2011. Electrical conductivity of continental lithospheric mantle from integrated geophysical and petrological modeling: application to the Kaapvaal Craton and Rehoboth Terrane, southern Africa. Journal of Geophysical Research — Solid Earth. American Geophysical Union.
Gallardo, L.A., Meju, M.A., 2003. Characterization of heterogeneous near-surface materials by joint 2D inversion of dc resistivity and seismic data. Geophysical Research Letters 30 (13).
Gallardo, L.A., Meju, M.A., 2004. Joint two-dimensional DC resistivity and seismic travel time inversion with cross-gradients constraints. Journal of Geophysical Research — Solid Earth 109 (B3).
Gokarn, S.G., Rao, C.K., Singh, B.P., Nayak, P.N., 1992. Magnetotelluric studies across the Kurduwadi gravity feature. Physics of the Earth and Planetary Interiors 72 (1–2), 58–67.
Groom, R.W., Bailey, R.C., 1989. Decomposition of magnetotelluric impedance tensors in the presence of local three dimensional galvanic distortion. Journal of Geophysical Research 94, 1913–1925.
Haak, V., Hutton, V.R.S., 1986. Electrical resistivity in continental lower crust. In: Dawson, J.B., Carswell, D.A., Hall, J., Wedepohl, K.H. (Eds.), The Nature of the Lower Continental Crust. Geological Society London, pp. 35–49.

Hyndman, R.D., Shearer, P.M., 1989. Water in the lower continental crust — modeling magnetotelluric and seismic reflection results. Geophysical Journal International 98 (2), 343–365.
Ilkisik, O.M., Jones, A.G., 1984. Statistical evaluation of MT and AMT methods applied to a basalt-covered area in southeastern Anatolia, Turkey. Geophysical Prospecting 32, 706–724.
Inman, J.R., 1975. Resistivity inversion with ridge regression. Geophysics 40 (5), 798–817.
Jagadeesh, S., Rai, S.S., 2008. Thickness, composition, and evolution of the Indian Precambrian crust inferred from broadband seismological measurements. Precambrian Research 162 (1–2), 4–15.
Jones, A.G., 1981. On a type classification of lower crustal layers under Precambrian regions. Journal of Geophysics-Zeitschrift fur Geophysik 49 (3), 226–233.
Jones, A.G., 1982. On the electrical crust–mantle structure in Fennoscandia: no Moho and the asthenosphere revealed? Geophysical Journal of the Royal Astronomical Society 68 (2), 371–388.
Jones, A.G., 1988. Static shift of magnetotelluric data and its removal in a sedimentary basin environment. Geophysics 53 (7), 967–978.
Jones, A.G., 1992. Electrical conductivity of the continental lower crust. In: Fountain, D.M., Arculus, R.J., Kay, R.W. (Eds.), Continental Lower Crust. Elsevier, pp. 81–143.
Jones, A.G., 1993. The COPROD2 dataset — tectonic setting, recorded MT data, and comparison of models. Journal of Geomagnetism and Geoelectricity 45 (9), 933–955.
Jones, A.G., 1999. Imaging the continental upper mantle using electromagnetic methods. Lithos 48 (1–4), 57–80.
Jones, A.G., 2012a. Distortion of magnetotelluric data: its identification and removal. In: Chave, A.D., Jones, A.G. (Eds.), The Magnetotelluric Method: Theory and Practice. Cambridge University Press, Cambridge (UK).
Jones, A.G., 2012b. Distortion decomposition of the magnetotelluric impedance tensors from a one-dimensional anisotropic Earth. Geophysical Journal International 268–284.
Jones, A.G., Ferguson, I.J., 2001. The electric Moho. Nature 409 (6818), 331–333.
Jones, A.G., et al., 2002. Magnetotelluric and teleseismic study across the Snowbird Tectonic Zone, Canadian Shield: a Neoarchean mantle suture? Geophysical Research Letters 29 (17).
Jones, A.G., Evans, R.L., Eaton, D.W., 2009a. Velocity–conductivity relationships for mantle mineral assemblages in Archean cratonic lithosphere based on a review of laboratory data and Hashin–Shtrikman extremal bounds. Lithos 131–143.
Jones, A.G., et al., 2009b. Area selection for diamonds using magnetotellurics: examples from southern Africa. Lithos 83–92.
Jones, A.G., Plomerova, J., Korja, T., Sodoudi, F., Spakman, W., 2010. Europe from the bottom up: a statistical examination of the central and northern European lithosphere–asthenosphere boundary from comparing seismological and electromagnetic observations. Lithos 120 (1–2), 14–29.
Jones, A.G., Fullea, J., Evans, R.L., Muller, M.R., 2012. Calibrating laboratory-determined models of electrical conductivity of mantle minerals using geophysical and petrological observations. Geochemistry Geophysics Geosystems. American Geophysical Union.
Jones, A.G., Fishwick, S., Evans, R.L., Muller, M.R., Fullea, J., 2013. Velocity–conductivity relations for cratonic lithosphere and their application: Example of Southern Africa. Geochemistry, Geophysics, Geosystems, 14, C10.1002/ggge.20075.
Karato, S.I., 1990. The role of hydrogen in the electrical conductivity of the upper mantle. Nature 347 (6290), 272–273.
Kariya, K.A., Shankland, T.J., 1983. Electrical conductivity of dry lower crustal rocks. Geophysics 48 (1), 52–61.
Ledo, J., Jones, A.G., Ferguson, I.J., Wolynec, L., 2004. Lithospheric structure of the Yukon, northern Canadian Cordillera, obtained from magnetotelluric data. Journal of Geophysical Research — Solid Earth, 109, B02403. http://dx.doi.org/10.1029/2002JB002305.
Maurer, H., Boerner, D.E., 1998. Optimized and robust experimental design: a non-linear application to EM sounding. Geophysical Journal International 132 (2), 458–468.
Maurer, H., Boerner, D.E., Curtis, A., 2000. Design strategies for electromagnetic geophysical surveys. Inverse Problems 16 (5), 1097–1117.
Maurer, H., Curtis, A., Boerner, D.E., 2010. Recent advances in optimized geophysical survey design. Geophysics 75 (5), A177–A194.
McPherron, R., 2005. Magnetic pulsations: their sources and relation to solar wind and geomagnetic activity. Surveys in Geophysics 26 (5), 545–592.
Mengel, K., Kern, H., 1992. Evolution of the petrological and seismic Moho — implications for the continental–crust mantle boundary. Terra Nova 4 (1), 109–116.
Mohorovičić, A., 1910. Godišnje izvješće zagrebačkog meteorološkog opservatorija za godinu 1909. Godina IX, dio IV. — polovina 1. Potres od 8. X, pp. 1–56.
Moorkamp, M., Jones, A.G., Eaton, D.W., 2007. Joint inversion of teleseismic receiver functions and magnetotelluric data using a genetic algorithm: are seismic velocities and electrical conductivities compatible? Geophysical Research Letters 34 (16).
Moorkamp, M., Jones, A.G., Fishwick, S., 2010. Joint inversion of receiver functions, surface wave dispersion, and magnetotelluric data. Journal of Geophysical Research — Solid Earth 115.
Parker, R.L., 1980. The inverse problem of electromagnetic induction: existence and construction of solutions based on incomplete data. Journal of Geophysics 85 (B8), 4421–4428.
Parker, R.L., 1984. The inverse problem of resistivity sounding. Geophysics 49 (12), 2143–2158.
Parker, R.L., Booker, J.R., 1996. Optimal one-dimensional inversion and bounding of magnetotelluric apparent resistivity and phase measurements. Physics of the Earth and Planetary Interiors 98 (3–4), 269–282.
Peslier, A.H., Woodland, A.B., Bell, D.R., Lazarov, M., 2010. Olivine water contents in the continental lithosphere and the longevity of cratons. Nature 467 (7311), 78–81.
Plotkin, V.V., Belinskaya, A.Y., Gavrysh, P.A., 2011. Nonlocal electromagnetic response: implications in the regional sounding. Izvestiya-Physics of the Solid Earth 47 (1), 23–32.
Qian, W., Boerner, D.E., 1992. Using a causal dispersion-relation to estimate phase from magnitude for controlled-source electromagnetic-field measurements. Geophysical Journal International 111 (2), 203–212.
Roux, E., Moorkamp, M., Jones, A.G., Lebedev, S., 2008. Joint inversion of magnetotelluric and surface waves data in anisotropic media. 19th EM Induction Workshop, Beijing, China.
Roy, A., Apparao, A., 1971. Depth of investigation in direct current methods. Geophysics 36 (5), 943–959.
Shalivahan, Bhattacharya, B.B., 2002. Implications of novel results about Moho from magnetotelluric studies. Current Science 83 (10), 1259–1264.
Shankland, T.J., Ander, M.E., 1983. Electrical conductivity, temperatures, and fluids in the lower crust. Journal of Geophysical Research 88 (NB11), 9475–9484.
Sharma, S.P., 2012. VFSARES — a very fast simulated annealing FORTRAN program for interpretation of 1-D DC resistivity sounding data from various electrode arrays. Computers & Geosciences 42, 177–188.
Smith, J.T., Booker, J.R., 1988. Magnetotelluric inversion for minimum structure. Geophysics 53 (12), 1565–1576.
Spratt, J.E., Jones, A.G., Nelson, K.D., Unsworth, M.J., 2005. Crustal structure of the India–Asia collision zone, southern Tibet, from INDEPTH MT investigations. Physics of the Earth and Planetary Interiors 150 (1–3), 227–237.
Spratt, J.E., Jones, A.G., Jackson, V.A., Collins, L., Avdeeva, A., 2009. Lithospheric geometry of the Wopmay orogen from a Slave Craton to Bear Province magnetotelluric transect. Journal of Geophysical Research — Solid Earth, 114, B01101. http://dx.doi.org/10.1029/2007jb005326.
Szalai, S., Novak, A., Szarka, L., 2009. Depth of investigation and vertical resolution of surface geoelectric arrays. Journal of Environmental and Engineering Geophysics 14 (1), 15–23.
Szaraniec, E., 1986. The inverse problem of resistivity sounding — comment. Geophysics 51 (5), 1151-1151.
ten Grotenhuis, S.M., Drury, M.R., Peach, C.J., Spiers, C.J., 2004. Electrical properties of fine-grained olivine: evidence for grain boundary transport. Journal of Geophysical Research — Solid Earth 109 (B6).
Thompson, D.A., et al., 2010. Precambrian crustal evolution: seismic constraints from the Canadian Shield. Earth and Planetary Science Letters 297 (3–4), 655–666.
van Zijl, J.S.V., Joubert, S.J., 1975. Crustal geoelectrical model for South African Precambrian granitic terrains based on deep Schlumberger soundings. Geophysics 40 (4), 657–663.
Velikhov, Y.P., et al., 1986. Electromagnetic studies on the Kola Peninsula and in Northern Finland by means of a powerful controlled source. Journal of Geodynamics 5, 237–256.
Wei, W., et al., 2008. Geoelectric structure of the lithosphere beneath Eastern North China: features of thinned lithosphere from magnetotelluric soundings. Earth Science Frontiers 15 (4), 204–216.
Wiggins, R.A., 1972. General linear inverse problem — implication of surface-waves and free oscillations for Earth structure. Reviews of Geophysics and Space Physics 10 (1), 251–285.
Yang, X.Z., 2011. Origin of high electrical conductivity in the lower continental crust: a review. Surveys in Geophysics 32 (6), 875–903.
Yardley, B.W.D., Valley, J.W., 1997. The petrologic case for a dry lower crust. Journal of Geophysical Research — Solid Earth 102 (B6), 12173–12185.
Yoshino, T., Noritake, F., 2011. Unstable graphite films on grain boundaries in crustal rocks. Earth and Planetary Science Letters 306 (3–4), 186–192.
Zhamaletdinov, A.A., 2011. The new data on the structure of the continental crust based on the results of electromagnetic sounding with the use of powerful controlled sources. Doklady Earth Sciences 438 (2), 798–802.
Zhamaletdinov, A.A., et al., 2009. International FENICS experiment on the tensor frequency electromagnetic sounding of the lithosphere in the Eastern Baltic (Fennoscandian) Shield. Doklady Earth Sciences 427 (2), 979–984.
Zhamaletdinov, A.A., et al., 2011. Deep electromagnetic sounding of the lithosphere in the Eastern Baltic (Fennoscandian) Shield with high-power controlled sources and industrial power transmission lines (FENICS Experiment). Izvestiya-Physics of the Solid Earth 47 (1), 2–22.